Comparison of Computational Methods of Associated Legendre Functions

Takeshi Enomoto
Disaster Prevention Research Institute, Kyoto University

Abstract

Comparisons are made between two computational methods for associated Legendre functions across truncation wave numbers between 39 and 10239. One of the two methods uses the four-point recurrence in double precision (the Fourier method) and the other uses the three-point recurrence in the extended arithmetic (the X-number method). Both methods avoid the shortcomings of the traditional method using the three-point recurrence in double precision and generate values accurate enough to enable stable Legendre transforms at large truncation wave numbers (> 1700). The errors for the Fourier method are found to be much smaller than those for the X-number method and have little latitudinal dependencies. The errors for the Fourier method, however, are found to grow rapidly with large degrees $n > 2048$. Two alternatives are proposed to calculate the scaling factor of the Fourier coefficients of the associated Legendre functions accurately with errors in $O(\sqrt{n})$.

(**Citation**: Enomoto, T., 2015: Comparison of computational methods of associated Legendre functions. *SOLA*, **11**, 144−149, doi:10.2151/sola.2015-033.)

1. Introduction

The spectral transform method (Orszag 1970; Bourke 1972, 1974; Hoskins and Simmons 1975) is widely used in numerical weather prediction (NWP) and climate models. The horizontal resolution of spectral models are indicated by the truncation wave number or the largest wave number in the expansion by spherical harmonics. Usually the zonal and total (zonal plus meridional) wave numbers are truncated at a same truncation wave number to give a uniform resolution over the globe. Recent increase in computing power allows the use of a large truncation wave number. With the advent of the Earth Simulator in 2002, simulations with T1279 (T for triangular truncation) using AFES (atmospheric general circulation model for the Earth Simulator) were conducted (Ohfuchi et al. 2004). The relation between the number of the grid in the zonal direction I and the truncation wave number in AFES is $I \geq 3N + 1$ due to the nonlinear advection terms (the quadratic grid) and for the above resolution $I = 3840$ and $N = 1279$, corresponding to 10-km resolution. Currently horizontal resolutions of 13−21 km are used in the operational NWP. The Japan Meteorological Agency increased the truncation wave number of the Global Spectral Model (GSM) for the deterministic forecasts from TL319 (L for the linear grid, where $I \geq 2N + 1$, 63 km) to TL959 (21 km) in 2007. Similarly, the European Centre for Medium-range Weather Forecasts increased from TL799 (50 km) to TL1279 (16 km) in 2010 and the National Centers for Environmental Prediction (NCEP) from T574 (23 km) to TL1534 (13 km) in 2015.

During the development of AFES, the AFES team became aware of the degradation of the Legendre transforms with increasing the truncation wave number: transforms with T1279 deteriorate to single precision and those with truncation wave numbers larger than 1700 fail. Enomoto et al. (2008) addressed this problem by using the four-point recurrence (Belousov 1962; Nehrkorn 1990; Swarztrauber 1993; Wedi et al. 2013) in place of the traditional three-point recurrence to compute the associated Legendre functions (ALFs).

Fukushima (2011) proposed an alternative method to compute ALFs using the three-point recurrence method in the extended arithmetic (X-number) based on Smith et al. (1981). Fukushima (2011) succeeded in reducing the overhead of the extended arithmetic to be additional 10% only by fusing the extended arithmetic addition and multiplication and embedding the X-number operations in the recurrence. The new method allows computation of ALFs at astonishingly large wave numbers up to $2^{32} \approx 4 \times 10^9$, which corresponds to a horizontal resolution of 3 and 5 mm on the quadratic and linear grids, respectively, for the Earth.

In this study, the four-point recurrence in double precision are compared with the three-point recurrence in the extended arithmetic in a practical range of T39−T10239. The three- and four-point recurrences are described in the next section. The results from computational tests are shown in Section 3. Finally, concluding remarks are given in Section 4.

2. Computational methods

In the spectral models, prognostic variable are expanded with spherical harmonics

$$Y_n^m(\lambda,\theta) = \tilde{P}_n^m(\cos\theta)e^{im\lambda} \tag{1}$$

where order m and degree n are the zonal and total wave numbers, respectively, λ and θ the longitude and colatitude, respectively, $\tilde{P}_n^m(\cos\theta)$ the normalized (quasi-normalized, in the geodesic literature) ALF, which is related with the unnormalized ALF $P_n^m(\cos\theta)$ by

$$\tilde{P}_n^m(\cos\theta) = \sqrt{\frac{2n+1}{2}\frac{(n-m)!}{(n+m)!}}P_n^m(\cos\theta) \tag{2}$$

for the normalization factor of 1 i.e.

$$\int_{-1}^{1}\left[\tilde{P}_n^m(\cos\theta)\right]^2 \mathrm{d}\cos\theta = 1. \tag{3}$$

The unnormalized ALF $P_n^m(\cos\theta)$ is defined by Rodrigues' formula

$$P_n^m(x) = \frac{(-1)^n}{2^n n!}(1-x^2)^{m/2}\frac{\mathrm{d}^{n+m}}{\mathrm{d}x^{n+m}}(1-x^2)^n \tag{4}$$

where $x = \cos\theta$. The values of $\tilde{P}_n^m(\cos\theta)$ are computed using one of recurrences described in the following two subsections at $J = I/2$ colatitudes θ, which are the zeros of $P_J(\cos\theta)$.

2.1 The three-point recurrence

The three-point recurrence may be written as

$$\tilde{P}_n^m(\cos\theta) = (a_n^m\cos\theta)\tilde{P}_{n-1}^m(\cos\theta) - b_n^m\tilde{P}_{n-2}^m(\cos\theta) \tag{5}$$

where

$$a_n^m = \sqrt{\frac{(2n-1)(2n+1)}{(n-m)(n+m)}},\quad b_n^m = \frac{a_n^m}{a_{n-1}^m}. \tag{6}$$

This recurrence involves the terms with the same zonal wave number but with different total wave numbers and requires two starting values for each zonal wave number

Corresponding author: Takeshi Enomoto, Disaster Prevention Research Institute, Kyoto University Gokasho, Uji, Kyoto 611-0011 Japan. E-mail: enomoto.takeshi.3n@kyoto-u.ac.jp. ©2015, the Meteorological Society of Japan.

$$\tilde{P}_m^m(\cos\theta) = (d_n^m \sin\theta)\tilde{P}_{m-1}^{m-1}(\cos\theta), \tag{7}$$

$$\tilde{P}_{m+1}^m(\cos\theta) = (a_{m+1}^m \cos\theta)\tilde{P}_m^m(\cos\theta) \tag{8}$$

where

$$d_n^m = \sqrt{\frac{2m+1}{2m}}. \tag{9}$$

The starting value $\tilde{P}_0^0(\cos\theta) = 1/\sqrt{2}$ for the normalization factor of 1. The recurrence (5) is illustrated in Fig. 1a. The value at the white circle is computed from the starting values at the filled circles. The starting values along the yellow lines ($n = m$ and $n = m + 1$) are pre-computed with (7) and (8), respectively.

Near the poles, the sectional harmonics ($m = n$) often have insufficient magnitude to be represented in floating-point formats. This is because a factor $\sin\theta$ is multiplied recursively whenever m gets larger in (7). Once the underflow occurs, it degrades all of the computed values of the successors in (5), (7) and (8), even if the true values of the successors in (5) have sufficient magnitudes.

2.2 The four-point recurrence

Swarztrauber (1993) suggested an alternative four-point recurrence (Fig. 1b). Its normalized version may be written as

$$\begin{aligned}\tilde{P}_n^m(\cos\theta) = &\sqrt{\frac{(2n+1)(n+m-3)(n+m-2)}{(2n-3)(n+m-1)(n+m)}}\tilde{P}_{n-2}^{m-2}(\cos\theta)\\ &-\sqrt{\frac{(n-m+1)(n-m+2)}{(n+m-1)(n+m)}}\tilde{P}_n^{m-2}(\cos\theta)\\ &+\sqrt{\frac{(2n+1)(n-m-1)(n-m)}{(2n-3)(n+m-1)(n+m)}}\tilde{P}_{n-2}^m(\cos\theta).\end{aligned} \tag{10}$$

This recurrence does not rely on the values at smaller degrees only but the values at a different order $m - 2$. As a consequence even when the values are growing with n and the values at small n are smaller than the minimum represented in double precision, the values are computed correctly because of the contribution from the terms at $m - 2$. Another consequence is that the values at $n - 2$ can be traced back to $\tilde{P}_n^0(\cos\theta)$ for even m and $\tilde{P}_n^1(\cos\theta)$ odd m.

The values at $m = 0$ ($\tilde{P}_n^0(\cos\theta)$) can be computed very accurately with the Fourier expansion of Legendre polynomials.

$$\tilde{P}_n(\cos\theta) = \sum_{k=0}^{n} a_{n,k}\cos k\theta \tag{11}$$

Because of this expansion, the four-point recurrence is referred to as *the Fourier method* hereafter.

The first few terms of this expansion can be obtained by expanding $(1 + 2h\cos\theta + h^2)^{-1}$ and collecting the coefficients of h^n to be

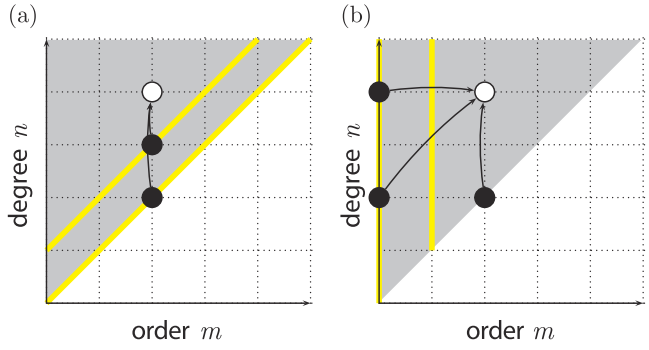

Fig. 1. Computation of associate Legendre functions with the (a) three- and (b) four-point recurrences. The values along the yellow lines are pre-computed before applying the recurrences.

$$\begin{aligned}\tilde{P}_n(\cos\theta) = &\sqrt{\frac{2n+1}{2}}2\frac{1\cdot3\cdot5\cdots(2n-1)}{2\cdot4\cdot6\cdots2n}\\ &\times\left[\cos n\theta + \frac{1\cdot n}{1\cdot(2n-1)}\cos(n-2)\theta\right.\\ &+\frac{1\cdot3}{1\cdot2}\frac{n(n-1)}{(2n-1)(2n-3)}\cos(n-4)\theta\\ &\left.+\frac{1\cdot3\cdot5}{1\cdot2\cdot3}\frac{n(n-1)(n-2)}{(2n-1)(2n-3)(2n-5)}\cos(n-6)\theta+\cdots\right].\end{aligned} \tag{12}$$

(a normalized form of (17) of Hobson 1931). The fact that $\tilde{P}_n(\cos\theta)$ is an even (odd) function for even (odd) n is consistent with this expansion composed of cosines of even (odd) multiples of θ. The values at $n = 1$ ($\tilde{P}_n^1(\cos\theta)$) are computed with the same coefficients in (12) using

$$P_n^1(\cos\theta) = -\frac{\mathrm{d}P_n(\cos\theta)}{\mathrm{d}\theta} \tag{13}$$

and the ratio of the normalizing factors of $\tilde{P}_n^1$ and $\tilde{P}_n^0$, $1/\sqrt{n(n+1)}$ (Belousov 1962).

The coefficient of $\cos n\theta$ may be written as

$$a_{n,n} = \sqrt{\frac{2n+1}{2}}\frac{(2n-1)!!}{2^{n-1}n!}. \tag{14}$$

It follows immediately from $a_{n,n}/a_{n-1,n-1}$

$$a_{n,n} = \sqrt{1-\frac{1}{4n^2}}a_{n-1,n-1}. \tag{15}$$

Swarztrauber (2002) suggested to calculate $a_{n,n}$ with (15). The starting value is $a_{1,1} = \sqrt{3/2}$ for the normalization factor of 1. However $1/4n^2$ in (15) quickly falls towards the machine epsilon (2.2204×10^{-16} for double precision) compared against 1. This problem can be avoided by rewriting (15) as

$$a_{n,n} = \frac{\sqrt{(2n-1)(2n+1)}}{2n}a_{n-1,n-1}. \tag{16}$$

Alternatively, (14) can be expressed in terms of the Gamma function $\Gamma(n + 1) \equiv n!$ as suggested by Swarztrauber (2002)

$$a_{n,n} = \sqrt{\frac{2n+1}{2}}\frac{\Gamma(2n+1)}{2^{2n-1}\Gamma^2(n+1)}. \tag{17}$$

Here the following asymptotic expansion is used

$$\begin{aligned}\Gamma(n+1) = n^n e^{-n}\sqrt{2\pi n}\left(1+\frac{1}{12n}+\frac{1}{288n^2}-\frac{139}{51840n^3}\right.\\ -\frac{571}{2488320n^4}+\frac{163879}{209018880n^5}\\ \left.+\frac{5246819}{75246796800n^6}-\frac{534703531}{902961561600n^7}+\cdots\right).\end{aligned} \tag{18}$$

Once $a_{n,n}$ is obtained the remaining $a_{n,k}$ are solved backwards with

$$l(2n-l+1)a_{n,n-l} - (l-1)(2n-l+2)a_{n,n-l+2} \tag{19}$$

where $l = n - k$ and $l = 2, 4, \ldots, n$ for even n and $l = 2, 4, \ldots, n - 1$ for odd n (Swarztrauber 2002).

The errors are compared among the original form (15) in Swarztrauber (2002), the one rewritten (16) and the one using the Gamma functions (17, 18) for $n = 2^i$, $i = 5, 6, \ldots, 20$ (Fig. 2). The error is measured by the maximum relative error

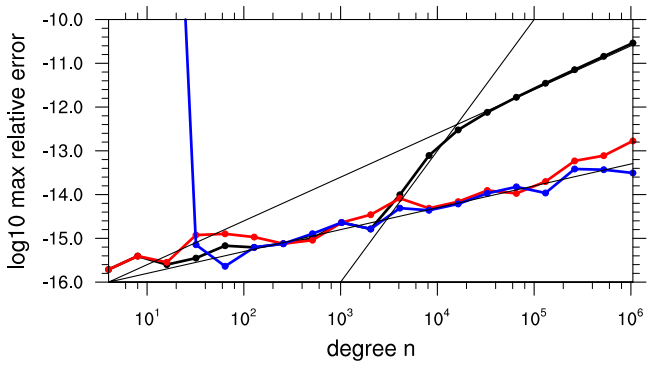

Fig. 2. The maximum relative error in the Fourier coefficients $a_{n,k}$ as computed from (15) in black, (16) in red and (17, 18) in blue. Thin black lines represent the slope for n^3, n and $\sqrt{n}$.

$$\mathrm{mr}(x_i) = \max_i \frac{|\epsilon(x_i)|}{|x_i|} \tag{20}$$

where x_i is a vector component and $\epsilon(x_i)$ its component error. The values computed with quadruple precision are regarded as the truth. The errors of the original form in black are in $O(\sqrt{n})$ up to 2^{11}, but suddenly grow rapidly in $O(n^3)$ between 2^{11} and 2^{14} and become proportional to $O(n)$ with $n \geq 2^{15}$. The errors in the rewritten form in red consistently follow $O(\sqrt{n})$, but the errors are often larger than those in the original form before the rapid increase. The errors in the form using the Gamma functions are smallest at many resolutions and comparable at the others except at small n, where the assumption of large n is inappropriate. It is suggested that the combination of the original form for small n and the form using the Gamma functions for large n should give the smallest errors.

2.3 The extended arithmetic

A non-zero floating-point number X is represented by a floating-point number x and an integer i as Fukushima (2011)

$$X = xB^i \tag{21}$$

where B is a large power on the base 2. Here $B = 2^{960}$ for double precision and $B = 2^{1600}$ for quadruple precision, proposed by Fukushima (2011), are used.

We call X normalized when

$$1/\sqrt{B} \leq |x| < \sqrt{B} \tag{22}$$

and weakly normalized when

$$1/B \leq |x| < B. \tag{23}$$

Normalization is applied to all the values in arithmetic operations when they are weakly normalized by dividing (multiplying) B and incrementing (decrementing) i to avoid overflow (underflow).

The extended arithmetic operations are applied to the three-point recurrence (5). The values are computed with the extended arithmetic and then stored in an array with double or quadruple precision. A small value (x/B) is used to represent the underflow values. Hereafter the three-point recurrence using the extended arithmetic is called *the X-number method*.

3. Computational tests

In this section, the X-number and Fourier methods are compared. The triangular truncation (signified by letter 'T' in front of the truncation wave number) and the quadratic grid are used in this study. The tests are conducted with various truncation wave numbers between T39 and T10239.

The Gaussian latitudes are computed as the zeros of P_J as a function of θ rather than that of $\cos\theta$ using the Newton method (Swarztrauber 2002). The Legendre polynomials are computed using the Fourier expansion (11, 12) without the scaling factor, which is irrelevant in finding the zeros. The Gaussian weights are obtained with

$$w(\theta) = \frac{2J+1}{\left[\tilde{P}'_J(\cos\theta) + \tilde{P}_J(\cos\theta)\cos\theta/\sin\theta\right]^2} \tag{24}$$

where $\tilde{P}'_J(\cos\theta) = \mathrm{d}\tilde{P}_J(\cos\theta)/\mathrm{d}\theta$ (Yakimiw 1996; Swarztrauber 2002). The Gaussian weights are computed using the Legendre polynomial and its derivative without scaling factor and are scaled so that $\sum_{j=0}^{J/2} w_j = 1$. As discussed in Enomoto et al. (2008), the errors of the Gaussian latitudes and weights are smaller with Legendre polynomials from the Fourier method described above than with those from the unnormalized version of the three-point recurrence (5) even at moderate resolutions (say T119).

3.1 Synthesis−analysis tests

In order to obtain the error for each wave number, synthesis−analysis tests are conducted. The initial value (and the truth) for each harmonics is 1. A Legendre synthesis followed by a Legendre analysis are conducted and the error is defined by

$$e_{\mathrm{sa}} = \left|1 - 2\sum_{j=1}^{J/2}\left[\tilde{P}_n^m(\cos\theta_j)\right]^2 w_j\right| \tag{25}$$

where $\tilde{P}_n^m(\cos\theta)$ is normalized to 1.

The errors for the X-number and Fourier methods are shown in Fig. 3. For T5119 both X-number and Fourier methods enable the accurate transforms at large n (Figs. 3a, b, respectively). Although the errors become larger with T10239 the X-number method seem to work robustly (Fig. 3d). The Fourier method, by contrast, (Fig. 3e) has large errors in small m increasing with n with the mean error 1.7 times larger than that of the X-number method. It is found that the cause of the errors is the original form for the scaling factor of the Fourier coefficient $a_{n,n}$ (15). Fortunately these error can be avoided with the modified form (16) or with the combination of (15) for $n \leq n_c$ and the Gamma functions (17, 18) for $n > n_c$ of $a_{n,n}$. Figure 3c and f show the tests using the latter with $n_c = 128$, which have slightly smaller errors than the modified form of (16).

With the fix of the scaling factor, the mean and maximum errors are smaller with the Fourier method than with the X-number method. This is probably because of the absence of the error accumulation in n due to the recurrence.

In the histograms of the errors with the X-number and Fourier methods (not shown), the most populated bins for the X-number and Fourier methods are $2-5 \times 10^{-14}$ and $1-2 \times 10^{-14}$, respectively. The errors are consistently smaller with the Fourier method in the maxima (the errors with Fourier method is 0.076−0.61 of those of the X-number method), means (0.48−0.63) and medians (0.42−0.67) of error (Table 1). Thus the errors with the Fourier method are roughly a half of those with the X-number method in the synthesis−analysis tests.

In order to complement the synthesis−analysis test, the orthogonality is measured for $n' \neq n$

$$e_{\mathrm{o}} = \left|\sum_{j=1}^{J/2} w(\theta_j)\tilde{P}_n^m(\cos\theta_j)\tilde{P}_{n'}^m(\cos\theta_j)\left[1+(-1)^{n+n'}\right]\right| \tag{26}$$

Due to enormous resource required for the computation of the orthogonality errors with a large truncation wave number, the errors computed for all m, $n \geq m$ and $n' \neq n$ for T1279 (Fig. 4) and an arbitrary combination of m and n for T2559. Figure 4 shows that the maximum of e_{o} does not have distinct dependency in m and the both methods are comparable in orthogonality although the Fourier method have slightly smaller errors. This is also the case for T2559; e_{o} for $n = 2500$ and $m = 1200$ are 3.22×10^{-14}, 1.81

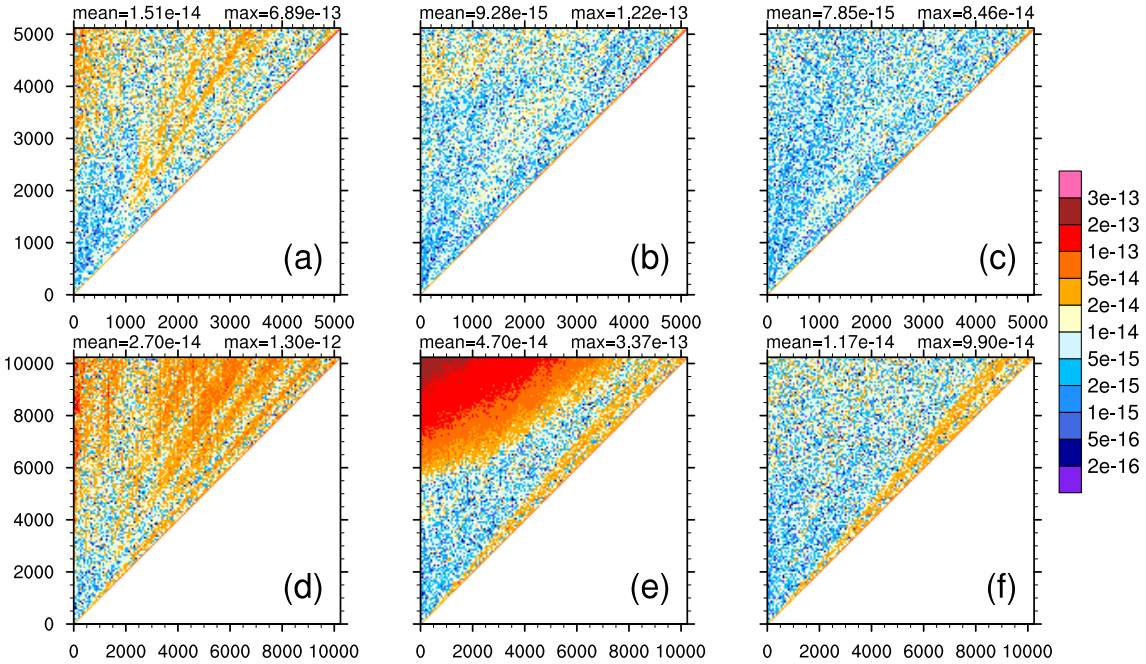

Fig. 3. Distribution of the error in the synthesis−analysis tests at T5119 (a, b, c) and at T10239 (d, e, f) with the X-number (a, d) and Fourier methods with the original form of the scaling factor $a_{n,n}$ (b, e) and the original form for total wave number for $n \leq 128$ and the form using the Gamma functions for $n > 128$ (c, f). The abscissa and ordinate denote order (zonal wave number) m and degree (total wave number) n, respectively.

Table 1. The maxima, means and medians of error in the synthesis−analysis tests at various resolutions with the X-number and Fourier methods

resolution	maximum		mean		median	
	X-number	Fourier	X-number	Fourier	X-number	Fourier
T39	7.77e-15	2.66e-15	1.14e-15	5.92e-16	8.88e-16	4.44e-16
T79	1.13e-14	3.77e-15	1.66e-15	8.08e-16	1.33e-15	6.66e-16
T119	1.04e-14	6.22e-15	1.76e-15	1.11e-15	1.33e-15	8.88e-16
T159	1.20e-14	7.33e-15	1.89e-15	1.18e-15	1.55e-15	8.88e-16
T239	3.93e-14	7.77e-15	2.71e-15	1.24e-15	2.00e-15	9.99e-16
T319	2.84e-14	1.11e-14	2.76e-15	1.60e-15	2.22e-15	1.33e-15
T639	5.97e-14	1.62e-14	4.49e-15	2.28e-15	3.55e-15	1.89e-15
T1279	1.21e-13	3.04e-14	6.73e-15	3.59e-15	5.11e-15	2.66e-15
T2559	1.76e-13	4.15e-14	1.34e-14	7.38e-15	1.13e-14	6.77e-15
T5119	6.89e-13	8.46e-14	1.51e-14	7.85e-15	1.18e-14	6.66e-15
T10239	1.30e-12	9.90e-14	2.70e-14	1.17e-14	2.13e-14	8.88e-15

$\times 10^{-14}$ and 1.51×10^{-16} for the X-number and Fourier methods and the three-term recurrence in quadruple precision, respectively.

3.2 Relative precision and identity error

Before examining the latitudinal distributions of errors, the numerical values for some combinations of n and m are compared (Supplement 1). The ALFs normalized to 1 are doubled in order to enable direct comparisons against those on Table 4 of Fukushima (2011) that shows the fully normalized ALF $\bar{P}_n^m(\cos\theta)$, normalized to 2 at $m = 0$ and to 4 at $m > 0$. The values computed using Maxima with 35 significant digits exactly agree with those computed using Mathematica by Fukushima (2011). The values computed using Fukushima (2011)'s and our implementations of the X-number method do not agree although the number of digits that agrees with the fixed precision calculation using Maxima or Mathematica is the same between the two implementations. In the combinations of m and n shown here, the values from the X-number and Fourier methods agree with those from Maxima in 10−12 digits. The agreements are extended to 30−31 digits with quadruple precision.

Now the relative precision against quadruple precision is examined. The relative precision is defined as

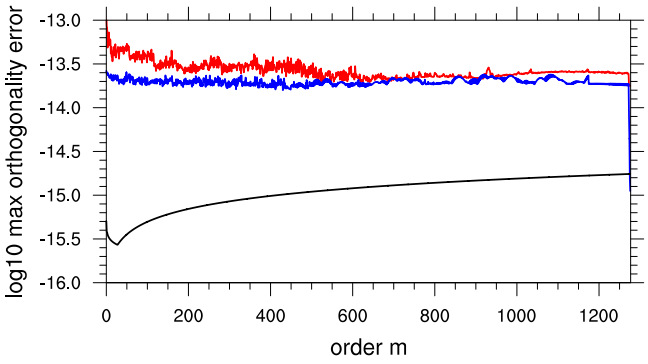

Fig. 4. The common logarithm of the maximum of the orthogonality errors for each m (ordinate) with the X-number (red), Fourier (blue) methods and the three-point recurrence in quadruple precision (black, not shifted) with T1279.

$$e_{\mathrm{rp}} = \frac{\delta A}{A_{\mathrm{r}}} \tag{27}$$

where δA and A_{r} are

$$\delta A \equiv \sum_{n=0}^{M}\sum_{m=0}^{n}\left|\tilde{P}_n^m(\cos\theta) - \hat{P}_n^m(\cos\theta)\right| \tag{28}$$

$$A_{\mathrm{r}} \equiv \sum_{n=0}^{M}\sum_{m=0}^{n}\left|\hat{P}_n^m(\cos\theta)\right| \tag{29}$$

where $\hat{P}_n^m(\cos\theta)$ is computed with the X-number method in quadruple precision, used as the proxy for the true value. The Kahan summation algorithm in quadruple precision is used in (28) and (29) to prevent the accumulation of round-off errors. Figure 5a shows the latitudinal distributions of relative precision for T10239. Both methods have relative precision of 12 digits except near the pole. The values at the closest point to the pole are 7.52×10^{-10} and 4.08×10^{-12} for the X-number and Fourier methods, respectively.

The relative precision may contain the systematic errors due to the properties of the recurrences. To supplement the relative precision, the accuracy is evaluated using an identity

$$I = \sum_{n=0}^{M}\sum_{m=0}^{n}\left[\bar{P}_n^m(\cos\theta)\right]^2 = (M+1)^2. \tag{30}$$

Again the Kahan summation algorithm is used in (30). The error is defined as

$$e_{\mathrm{id}} = \left|\frac{I-(M+1)^2}{(M+1)^2}\right| \tag{31}$$

(Holmes and Featherstone 2002).

The identity errors are oscillating around 1×10^{-15} with the Fourier method (Fig. 5b). The errors are larger with the X-number method by two orders of magnitude. In addition, there is a sharp increase of error near the pole. The latitudinal distribution of identity error suggests that even when the extended arithmetic is used the the three-point recurrence are less accurate than the four-point recurrence, especially near the pole. This is due to the three-point recurrence as suggested by the similar curve of quadruple precision (note the shift by 20 digits). It is worth restating that the X-number method is used to avoid underflow or overflow and it cannot change the characteristics of the recurrence. The identity errors might affect the relative precision of the Fourier method near the pole.

Figure 6 shows the resolution dependency of the relative precision and identity error. The maximum relative precision (solid) is increasing is faster than the mean (broken), suggesting the influence of error near the pole. The X-number methods in double and quadruple precision share the similar rates of growth in identity error. The Fourier methods, by contrast, shows a remarkably slow growth in identity error.

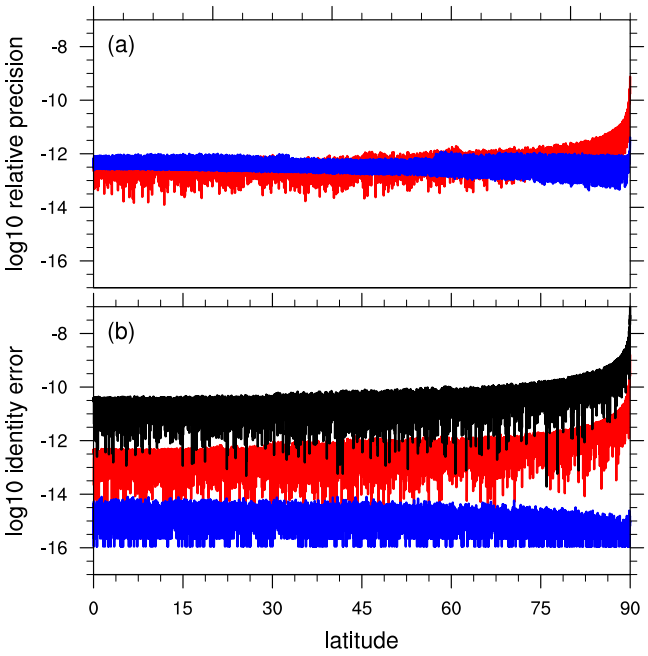

Fig. 5. Latitudinal distribution of the common logarithms of (a) the relative precision against the X-number method in quadruple precision and (b) the identity errors (see the definition in the text) with the X-number (red) and with the Fourier (blue) methods with T10239. The black curve in (b) shows the common logarithm of the identity error with the X-number method in quadruple precision shifted by 20.

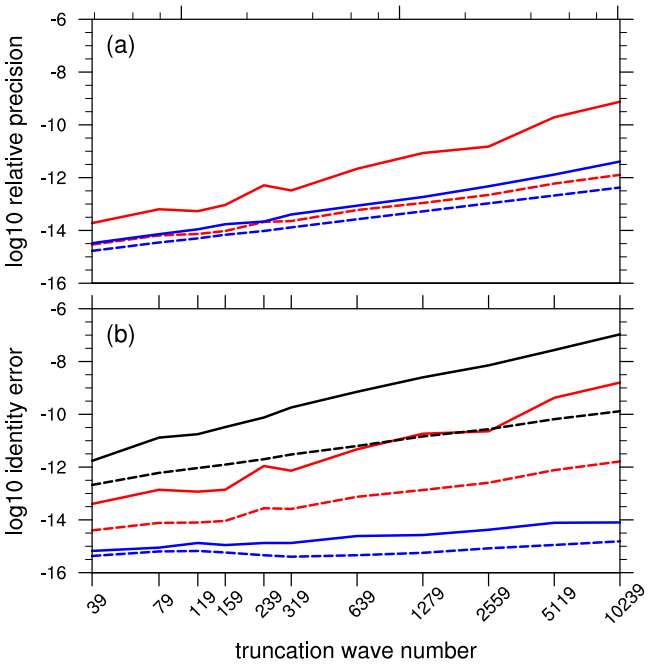

Fig. 6. As in Fig. 5 but the resolution dependency of the maximum (solid) and the mean (broken) of the common logarithms

4. Concluding remarks

The associate Legendre functions (ALFs) cannot be computed accurately with the three-point recurrence in double precision for large degrees and orders. Two alternatives are the three-point recurrence using the extended arithmetic (the X-number method) and the four-point recurrence in double precision with Legendre polynomials $\tilde{P}_n(\cos\theta)$ expanded in the Fourier series (the Fourier method). Both methods allow stable Legendre transforms at high resolutions. The Fourier method has been implemented in AFES (Enomoto et al. 2008) and in ECMWF IFS (Integrated Forecast System, Wedi et al. 2013). The X-number method has been implemented experimentally in NCEP GSM to result in a positive impact in forecast skills (Han-Ming Henry Juang 2012, *pers. comm.*) and adopted for operational use in TL1534.

In the Fourier method the scaling factor of the Fourier coefficients become less accurate at large degrees with the original form proposed by Swarztrauber (2002). Two alternatives are proposed and used in the computational tests in the present paper.

Computational tests show that Legendre transforms using the Fourier method are more accurate than those using the X-number method. In addition the errors with the X-number method have a sharp increase of error towards the pole.

The X-number method has advantages in speed. The time in seconds required to compute ALF is compared with a serial program on Mac Pro 2013 with 3.5 GHz 6-core Intel Xeon E5 and 32 GB memory (Supplement 2). The time grows in proportion to the cube of the truncation wave number. The X-number method is several time faster than the Fourier method, an order of magnitude faster than quadruple precision. The overhead due to extended arithmetic operations is negligible. Moreover, the three-point recurrence, which is independent in order m, allows the parallelization in m. The four-point recurrence, on the hand, requires the values at $m - 2$ and cannot be parallelized in m. As a result the computation can be slower although it has to be done only once in the initialization step.

The Fortran modules to compute ALFs used in this study are a part of enomo, available from http://github.com/tenomoto/enomo.

Acknowledgments

This work was supported by JSPS KAKENHI Grant Number 15K13417. The NCAR Command Language 6.3.0 (UCAR, 2015) was used for analysis and visualization. Maxima 5.36.1 was used to calculate the coefficients of the asymptotic series for the Gamma function. GNU Awk 4.1.3 with MPFR 3.1.3 was used in the error analysis of the Fourier method. To compile the Fortran source code, g95 0.93 and gfortran 5.2.0 were used. The author thanks Dr Kengo Miyamoto for useful suggestions and for thorough comments on the first draft. The author also appreciates the constructive comments from the Editor Dr Kazuo Saito and two anonymous reviewers.

Edited by: K. Saito

Supplments

Supplementary materials include a table and a figure.

References

Belousov, S. L., 1962: *Tables of Normalized Associated Legendre Polynomials*, Pergamon Press, New York.

Bourke, W., 1972: An efficient, one-level, primitive-equation spectral model. *Mon. Wea. Rev.*, **100**, 683−689.

Bourke, W., 1974: A multi-level spectral model. i. formulation and hemispheric integrations. *Mon. Wea. Rev.*, **102**, 687−701.

Enomoto, T., A. Kuwano-Yoshida, N. Komori, and W. Ohfuchi, 2008: Description of AFES 2: Improvements for high-resolution and coupled simulations. *High Resolution Numerical Modelling of the Atmosphere and Ocean*, K. Hamilton and W. Ohfuchi, Eds., Springer New York, chap. 5, 77−97.

Fukushima, T., 2011: Numerical computation of spherical harmonics by extending exponent of floating point numbers. *J. Geodesy*, **86**, 271−285.

Hobson, E. W., 1931: *The Theory of Spherical and Ellipsoidal Harmonics*, Cambridge University Press, Cambridge, UK.

Holmes, S. A., and W. E. Featherstone, 2002: A unified approach to the Clenshaw summation and the recursive computation of very high degree and order normalised associated legendre functions. *J. Geodesy*, **76**, 279−299.

Hoskins, B. J., and A. J. Simmons, 1975: A multi-layer spectral model and the semi-implicit method. *Quart. J. Roy. Meteor. Soc.*, **101**, 637−655.

Nehrkorn, T., 1990: On the computation of Legendre functions in spectral models. *Mon. Wea. Rev.*, **118**, 2248−2251.

Ohfuchi, W., co-authors, 2004: 10-km mesh meso-scale resolving simulations of the global atmosphere on the Earth Simulator ―preliminary outcomes of AFES (AGCM for the Earth Simulator)―. *J. Earth Simulator*, **1**, 8−34.

Orszag, S. A., 1970: Transform method for the calculation of vector-coupled sums: application ot the spectral form of the vorticity equation. *J. Atmos. Sci.*, **27**, 890−895.

Smith, J. M., F. W. Oliver, and D. W. Lozier, 1981: Extended-range arithmetic and normalized Ledendre polynomials. *J. ACM. Trans. Math. Software*, **7**, 93−105.

Swarztrauber, P. N., 1993: The vector harmonic transform method for solving partial differential equations in spherical geometry. *Mon. Wea. Rev.*, **121**, 3415−3437.

Swarztrauber, P. N., 2002: On computing the points and weights for gauss−legendre quadrature. *SIAM J. Sci. Comput.*, **24**, 945−954.

Yakimiw, E., 1996: Accurate computation of weights in classical Gauss-Cristoffel quadrature rules. *J. Comp. Phys.*, **192**, 406−430.

Wedi, N. P., M. Hamrud, and G. Mozdzynski, 2013: A fast spherical harmonics transform for global NWP and climate models. *Mon. Wea. Rev.*, **141**, 3450−3461.

Manuscript received 14 August 2015, *accepted 16 October 2015*
SOLA: *https://www.jstage.jst.go.jp/browse/sola/*